

Segmentation of subcortical brain structures using fuzzy templates

Juan Zhou and Jagath C. Rajapakse*

Bioinformatics Research Center, School of Computer Engineering, Nanyang Technological University, Block N4, 50 Nanyang Avenue, Singapore 639798

Received 15 January 2005; revised 16 June 2005; accepted 28 June 2005
Available online 2 August 2005

We propose a novel method to automatically segment subcortical structures of human brain in magnetic resonance images by using fuzzy templates. A set of fuzzy templates of the structures based on features such as intensity, spatial location, and relative spatial relationship among structures are first created from a set of training images by defining the fuzzy membership functions and by fusing the information of features. Segmentation is performed by registering the fuzzy templates of the structures on the test image and then by fusing them with the tissue maps of the test image. The final decision is taken in order to optimize the certainty in the intensity, location, relative position, and tissue content of the structure. Our method does not require specific expert definition of each structure or manual interactions during segmentation process. The technique is demonstrated with the segmentation of five structures: thalamus, putamen, caudate, hippocampus, and amygdala; the performance of the present method is comparable with previous techniques.

© 2005 Elsevier Inc. All rights reserved.

Introduction

Magnetic resonance imaging (MRI) is able to provide a detailed information of normal and diseased anatomy for medical research and has become a significant imaging modality in clinical diagnosis and treatment planning. Segmentation of subcortical structures from MR brain scans is a critical task that has numerous applications such as quantitative morphometry, 3D volume visualization, mapping brain structures and functions, and clinical investigations including pathology, diagnosis, therapy, surgery planning, etc. Manual segmentation is time-consuming, subjective, and error prone; inter- or intra-observer variability may reduce the ability to detect subtle differences during comparisons. Moreover, the growing size and number of MR images have necessitated the use of computers to facilitate automatic segmentation (Pham et al., 2000; Sonka and Fitzpatrick, 2000).

There are a few main issues that should be addressed by any automatic subcortical structure segmentation technique. The inhomogeneous intensity within one tissue class or structure and

the overlapping intensity characteristics among different structures may reduce the effectiveness of intensity-based methods (Rajapakse et al., 1997). Although the spatial information can be incorporated to solve the inherent ambiguities of class intensity distributions, due to the complexity and variability of the shape, size, and orientation, accurate identification of brain anatomical structures is a challenging task. Other issues such as low contrast, noise perturbation, partial volume effect, and scanner magnetic field inhomogeneities of MR images should also be addressed (Sonka and Fitzpatrick, 2000; Xue et al., 2000).

A wide variety of methods have been proposed in the literature for segmentation of subcortical structures (Pham et al., 2000). Deformable models, which deform a template based on the extracted image features, have been extensively studied and widely used in medical image segmentation with promising results (Sonka and Fitzpatrick, 2000). However, it relies on human experts for initialization and guidance, and intelligent optimization algorithms are required to automate the approach. Prior knowledge such as atlases is helpful to the segmentation process, so elastic image registration techniques based on atlases were proposed to identify brain structures (Kelemen et al., 1999). However, the accuracy of registration mechanism largely influences the segmentation performance. Bayesian approach has been applied to detect a number of neuroanatomical structures (Fischl et al., 2002). A set of manually labeled training images is used to create probabilistic prior maps of the structure of interests by a linear registration to the atlas and a test image is segmented by the maximum a posteriori (MAP) estimation based on some assumptions. Knowledge-based approaches such as fuzzy modeling (Xue et al., 2000) and information fusion (Barra and Boire, 2001) have also been adopted. Hybrid techniques were also proposed to further increase the accuracy of detection, such as maximum a posterior estimation of structures with level set prior information (Yang et al., 2004), combining fuzzy clustering technique with deformable models for thalamus segmentation (Amini et al., 2004), and fitting a group of deformable templates supervised by a series of rules derived from analyzing the template's dynamics and expert knowledge (Pitiot et al., 2004). Shape descriptors such as moments of 3D coordinates are recently proposed to characterize brain structure morphometry (Mangin et al., 2004). Other approaches include histogram analysis (Worth et al., 1998), neural network techniques (Magnotta et al., 1999), and genetic algorithms (Sonka et al., 1996). Despite all

* Corresponding author.

E-mail address: asjagath@ntu.edu.sg (J.C. Rajapakse).

Available online on ScienceDirect (www.sciencedirect.com).

these efforts, due to the unavailability of efficient and accurate automatic segmentation methods that are suitable for clinical use, clinicians still rely on manual segmentation of subcortical brain structures from MR images. There is a need to further investigate into novel techniques that can automatically detect the subcortical structures more accurately.

We approach the problem of segmentation of subcortical structures by (1) incorporating the spatial information of structures as intensity is not enough for reliable estimation of structures, (2) taking into consideration the predictable spatial relationships among structures although individual variability exists in terms of shape, orientation, and location of the structures, and (3) using a set of training images to obtain prior information of each structure of interest in the form of fuzzy templates as the information provided by the test image and a single rigid template is incapable of handling the individual variability of the structures.

The expert knowledge such as “the putamen was defined as a gray matter prismatic-shaped structure, located approximately at 25 mm of the lateral ventricles, almost symmetric with respect to the inter-hemispheric plane and slightly posterior to the frontal horn of the lateral ventricles” may be useful for the segmentation of a certain structure (Barra and Boire, 2001). But this kind of expert definition of brain subcortical structure may be vague, different experts may come out with slightly different definitions; some parameters like “25 mm” may not be suitable for a different group of subjects. Therefore, the present approach does not require expert definitions, instead, it automatically extracts the prior knowledge of the target structure from a set of manually segmented training images and encodes them into fuzzy templates. On the other hand, atlas-based approaches usually represent the prior knowledge by a rigid template, which cannot take into account the variability of individual anatomy. As a result, we are motivated to use fuzzy logic to model anatomical variability and demonstrate that fuzzy templates would be a useful way to represent prior knowledge about subcortical structures.

In order to manage the imprecision and the uncertainty inherent in the structures, fuzzy templates of different subcortical structures in terms of different features such as intensity, spatial location, relative distance, and relative direction are first created and fused based on a set of training images under the fuzzy logic framework. The fuzzy templates are then used as the prior knowledge for segmentation by nonlinearly registering with the test image. Secondly, the tissue information of the test image is fused together with the fuzzy templates to form a fuzzy map of different structures. A defuzzification step with α -cut on fuzzy maps is finally used to clearly identify the location and boundary of subcortical structures. Experiments with the detection of five subcortical structures: thalamus, caudate, putamen, hippocampus, and amygdala, on 17 images are presented; the results were compared with previous approaches.

Method

The first step in our method is to construct fuzzy templates from the features of each structure; a set of training images normalized to a standard template is used for this purpose. Fuzzy maps of each structure for the test image are then created by registering and fusing the fuzzy templates with the tissue maps of the test image. The final detection is made by a defuzzification step.

Construction of fuzzy templates

Suppose that there is a standard template $r = (r_i: i \in B)$ of human brain B , where r_i is the image intensity at the voxel site i of the template r . We have a set of N real value 3D MR brain images, $F = \{f^j: j = 1, 2, \dots, N\}$ along with their expert segmentations to learn the fuzzy templates of the structures. The j th training image is denoted by $f^j = (f_i^j: i \in I)$ where f_i^j is the image intensity of the voxel i in the image f^j and $I \subset \mathbb{N}^3$ is the set of coordinates of the voxels in the domain of image f^j . Suppose that the expert segmentation identifies L number of structures indexed by the set $\Gamma = \{1, 2, \dots, L\}$ from each image; the labeled image (expert segmentation) corresponding to the image f^j is denoted by $s^j = (s_i^j = l: i \in I, l \in \Gamma)$, where the voxel site i in image f^j belongs to the structure l .

Normalization

In order to construct fuzzy templates based on a set of training images, we need to normalize all training images $F = \{f^j: j = 1, 2, \dots, N\}$ to a standard template r to create a set of normalized images $\tilde{F} = \{\tilde{f}^j: j = 1, 2, \dots, N\}$, which standardizes all brain scans to same size and orientation under the same coordinate system. We apply 12-parameters affine transformation followed by nonlinear warping for normalization (Ashburner and Friston, 1999). The optimal 12 parameters for registration can be computed by Gauss–Newton optimization algorithm as described in Friston et al. (1995). Nonlinear warping based on a linear combination of discrete cosine transform (DCT) basis functions is applied to correct gross differences in head shapes. This optimization is extended to maximum a posterior (MAP) solution to incorporate the prior knowledge for regularization (Ashburner et al., 1997). The same transformation computed from normalizing training images f^j to the template r is applied to each image’s expert segmentation s^j to obtain a set of normalized segmented images $\tilde{s}^j = (\tilde{s}_i^j = l: i \in I, l \in \Gamma)$ where $j = 1, 2, \dots, N$.

Fuzzy feature maps

For each pair of normalized segmentation \tilde{s}^j and normalized image \tilde{f}^j , there are L groups of voxels that belong to different structures $l \in \Gamma$. Let us denote the set of voxels belonging to the structure l in the normalized image \tilde{f}^j as $G_j^l = (i: \tilde{s}_i^j = l, i \in I)$. For each structure $l \in \Gamma$, three fuzzy feature maps for each image $\tilde{f}^j \in \tilde{F}$ are created:

Intensity. We model the structure l in the normalized training image \tilde{f}^j as a fuzzy set based on its intensity characteristics and its fuzzy membership function is directly estimated from the intensity histogram of G_j^l . Then, an intensity fuzzy map for the structure l corresponding to the normalized training image \tilde{f}^j is created. For every voxel i in the normalized training image \tilde{f}^j , the fuzzy membership A_{ij}^l for structure l is calculated from normalized training image \tilde{f}^j and segmentation \tilde{s}^j as follows:

$$A_{ij}^l = \begin{cases} \frac{H^l(i, l, j) - H_{\min}^l(l, j)}{2(H_{\max}^l(l, j) - H_{\min}^l(l, j))} + 0.5 & \text{if } \tilde{s}_i^j = l; \\ 0 & \text{otherwise,} \end{cases}$$

where $H^l(i, l, j)$ represents the number of voxels in G_j^l having the same intensity as voxel i in image \tilde{f}^j ; $H_{\min}^l(l, j) = \min_i H^l(i, l, j)$ and $H_{\max}^l(l, j) = \max_i H^l(i, l, j)$ stand for the minimum and maximum number of voxels having the same intensity in G_j^l , respectively. Thus, for voxels belonging to G_j^l , its intensity fuzzy

membership is in the range [0.5, 1] depending on its value in the histogram, otherwise zero fuzzy membership value is assigned. The above fuzzy membership function is designed to differentiate largely between those voxels belonging to this structure and other voxels, and to give higher fuzzy memberships to more prominent voxels and lower values to less prominent ones based on the intensity distribution of a particular structure.

Spatial location. Suppose x_{ij} , y_{ij} , and z_{ij} stand for the voxel i 's spatial location in the normalized image \tilde{f}^j as from left to right, from posterior to anterior, from inferior to superior. The spatial location of structure l in \tilde{f}^j can be modeled by a three-dimensional fuzzy map based on histograms of x , y , and z values for all voxels in the structure. Similar to the intensity fuzzy membership function, spatial location fuzzy membership functions in one direction D is defined as:

$$B(D)_{ij}^l = \begin{cases} \frac{H^D(i,l,j) - H_{\min}^D(l,j)}{2(H_{\max}^D(l,j) - H_{\min}^D(l,j))} + 0.5 & \text{if } \tilde{s}_i^j = l; \\ 0 & \text{otherwise,} \end{cases}$$

where $D \in \{x, y, z\}$ stands for the three directions, $H^D(i, l, j)$ is the number of voxels in G_j^l having the same spatial location value in the direction D as voxel i in image \tilde{f}^j , $H_{\min}^D(l, j) = \min_i H^D(i, l, j)$, and $H_{\max}^D(l, j) = \max_i H^D(i, l, j)$. The combination of these three fuzzy memberships produces a value of each voxel i in the spatial location fuzzy map of each structure l in each image \tilde{f}^j as:

$$B_{ij}^l = \sqrt[3]{B(x)_{ij}^l B(y)_{ij}^l B(z)_{ij}^l} \quad (3)$$

Relative spatial relations. Since the topological information of subcortical structures in human brain is important and predictable, relative spatial relations between structure G_j^l , $l \in \Gamma$ and other structures $G_j^{l'}, l' (\neq l) \in \Gamma$ in j th normalized training image can be expressed in terms of a relative spatial relation fuzzy map based on relative distance $C(\text{dis})_{ij}^{ll'}$ and relative direction $C(\text{dir})_{ij}^{ll'}$ with respect to some structures. Again, the fuzzy memberships are estimated from the distance and direction histograms. Let $d_{ij}^{ll'} = \|i - o_j^{l'}\|$ stand for the distance between voxel i in image \tilde{f}^j and $o_j^{l'}$ which is the centroid of the structure l' in image \tilde{f}^j . The relative distance fuzzy map is given by:

$$C(\text{dis})_{ij}^{ll'} = \begin{cases} \frac{H^{\text{dis}}(d_{ij}^{ll'}, l', l, j) - H_{\min}^{\text{dis}}(l', l, j)}{2(H_{\max}^{\text{dis}}(l', l, j) - H_{\min}^{\text{dis}}(l', l, j))} + 0.5 & \text{if } \tilde{s}_i^j = l; \\ 0 & \text{otherwise,} \end{cases} \quad (4)$$

where $H^{\text{dis}}(d_{ij}^{ll'}, l', l, j)$ is number of voxels in G_j^l having same distance $d_{ij}^{ll'}$ to the centroid $o_j^{l'}$ of structure l' in image \tilde{f}^j from voxel i ; $H_{\min}^{\text{dis}}(l', l, j)$ and $H_{\max}^{\text{dis}}(l', l, j)$ denote the minimum and maximum number of voxels in G_j^l with the same distance to centroid $o_j^{l'}$ of structure l' in image \tilde{f}^j , respectively.

As defined above, there are three directions x , y , and z , in a 3D MR image. A vector is formed from the centroid of one structure $o_j^{l'}$ to certain voxel i in image \tilde{f}^j and its direction in three-dimensional space can be decided by three angles with xy plane ($z = 0$), xz plane ($y = 0$), and yz plane ($x = 0$), respectively as:

$$\alpha(xy)_{ij}^{ll'} = \begin{cases} \arcsin\left(\frac{(i - o_j^{l'}) * (0 \ 0 \ 1)}{\|i - o_j^{l'}\|}\right) \frac{180}{\pi} & \text{if } \tilde{s}_i^j = l; \\ 0 & \text{otherwise;} \end{cases} \quad (5)$$

$$\alpha(yz)_{ij}^{ll'} = \begin{cases} \arcsin\left(\frac{(i - o_j^{l'}) * (1 \ 0 \ 0)}{\|i - o_j^{l'}\|}\right) \frac{180}{\pi} & \text{if } \tilde{s}_i^j = l; \\ 0 & \text{otherwise;} \end{cases} \quad (6)$$

$$\alpha(xz)_{ij}^{ll'} = \begin{cases} \arcsin\left(\frac{(i - o_j^{l'}) * (0 \ 1 \ 0)}{\|i - o_j^{l'}\|}\right) \frac{180}{\pi} & \text{if } \tilde{s}_i^j = l; \\ 0 & \text{otherwise;} \end{cases} \quad (7)$$

where $*$ indicates the inner product of the two vectors. The range of the above angles are $[-90, 90]$ and the direction fuzzy memberships of each voxel i in image \tilde{f}^j is given by

$$C(\text{dir})_{ij}^{ll'} = \sqrt[3]{\prod_{\psi \in \{xy, yz, xz\}} C(\psi)_{ij}^{ll'}} \quad (8)$$

where the form of the fuzzy membership function is same for three angles, $\psi \in \{xy, yz, xz\}$ as below:

$$C(\psi)_{ij}^{ll'} = \begin{cases} \frac{H^\psi(\alpha(\psi)_{ij}^{ll'}, l, l', j) - H_{\min}^\psi(l, l', j)}{2(H_{\max}^\psi(l, l', j) - H_{\min}^\psi(l, l', j))} + 0.5 & \text{if } \tilde{s}_i^j = l; \\ 0 & \text{otherwise,} \end{cases} \quad (9)$$

where $H^\psi(\alpha(\psi)_{ij}^{ll'}, l, l', j)$ is the number of voxels in G_j^l having the same angle $\alpha(\psi)_{ij}^{ll'}$ as voxel i to centroid $o_j^{l'}$ of structure l' with respect to direction ψ in image \tilde{f}^j ; $H_{\min}^\psi(l, l', j) = \min_i H^\psi(\alpha(\psi)_{ij}^{ll'}, l, l', j)$ and $H_{\max}^\psi(l, l', j) = \max_i H^\psi(\alpha(\psi)_{ij}^{ll'}, l, l', j)$.

After obtaining fuzzy maps $C(\text{dis})_{ij}^{ll'}$ (relative distance) and $C(\text{dir})_{ij}^{ll'}$ (relative direction) for structure l with respect to every other structure l' in \tilde{f}^j , a total relative spatial relations fuzzy map can be fused in two steps. For each voxel i in \tilde{f}^j , we first combine relative distance and relative direction for structure l with respect to one structure l' , and then fuse over all reference structures l' , ($l' \neq l$), to produce a new fuzzy membership C_{ij}^l . T-norm fusion operator is used since an overlap of information is desired.

$$C_{ij}^{ll'} = \sqrt{C(\text{dis})_{ij}^{ll'} * C(\text{dir})_{ij}^{ll'}} \quad (10)$$

$$C_{ij}^l = \sqrt[l-1]{\prod_{l'=1, l' \neq l} C_{ij}^{ll'}} \quad (11)$$

In this way, every training image will have three fuzzy maps for each structure $l \in \Gamma$ based on intensity, spatial location, and relative spatial relations: A_{ij}^l , B_{ij}^l , and C_{ij}^l where $i \in I$ and $j = 1, 2, \dots, N$. Note that the final fuzzy membership of each voxel in every fuzzy map should be in the range [0.5, 1] for true belonging. In this way, we can differentiate the true voxels from the others more accurately for each structure in each image and better prepare the maps for the next fusion step to create the fuzzy templates of the structures.

Information fusion

Three kinds of features—intensity A , spatial location B , and relative spatial relations C —have been modeled by fuzzy membership functions for each training image. The fuzzy feature maps of all training images are fused to obtain fuzzy feature templates and a total fuzzy template involving all features for different structures.

A simple mean fusion operator is used to produce average fuzzy memberships of structure l for each voxel $i \in I$, across all training images:

$$W_i^l = \frac{1}{N} \sum_{j=1}^N W_{ij}^l \quad (12)$$

where $W = \{A, B, C\}$ represents intensity, spatial location, and relative spatial relations, respectively. As a result, three fuzzy feature templates $A^l = (A_i^l: i \in I)$, $B^l = (B_i^l: i \in I)$, and $C^l = (C_i^l: i \in I)$ were constructed for each structure of interests $l \in \Gamma$. Further, information fusion is possible to form a total fuzzy template $T^l = (T_i^l: i \in I)$ to include all three fuzzy features as:

$$T_i^l = \left(\left(A_i^l * B_i^l \right)^{0.5} * C_i^l \right)^{0.5} \quad (13)$$

We first combine intensity and spatial locations, and then with relative spatial relations. The reason for doing this two-step fusion is to first consider overlapped information based on intensity and location of all voxels belonging to structure l itself. Then, secondly, relative spatial relations feature template, which is based on spatial location of voxels both in structure l and other structures, is fused to further refine the information of structure l accurately.

Segmentation

A three-steps scheme is described below to segment a given test image f into different structures $l \in \Gamma$ based on the fuzzy templates A^l, B^l, C^l , and T^l constructed using the training images.

Registration

In order to make use of the fuzzy templates created during training, the fuzzy membership information must be made available to each voxel in the test image f . Registration from the fuzzy templates to the test image is done by using the same method as in the training stage but in the reverse direction. As a result, all voxels in the test image f have prior fuzzy memberships to structure $l \in \Gamma$ based on the registered fuzzy features denoted as \tilde{A}_i^l for intensity, \tilde{B}_i^l for spatial location, \tilde{C}_i^l for relative spatial relation, and \tilde{T}_i^l for total information.

Incorporation of tissue information

The brain matter can be broadly classified into gray matter (GM), white matter (WM), and cerebrospinal fluid (CSF). Different subcortical structures have different tissue properties, which information is proved to be useful for segmentation (Barra and Boire, 2001). Therefore, fuzzy maps of three tissue classes $k \in \{GM, WM, CSF\}$ are constructed to grasp more unique properties of different structures in the test image f such as shape, size, and orientation, which may not be handled satisfactorily by the registered fuzzy templates only.

There are many approaches for tissue segmentation and we used the approach proposed by (Ashburner and Friston, 1997). It is an extension of a clustering algorithm, the maximum likelihood mixture model algorithm, by incorporating a prior spatial probability map of belonging to each tissue type and a correction of image intensity nonuniformity by using a Bayesian model. The process starts by estimating probabilities of each tissue class based on a priori map and then iteratively computes cluster parameters, belonging probabilities, and sensitivity fields from intensity corrected images until a convergence criterion is satisfied (Ashburner and Friston, 1997, 2000). It uses a mixture of Gaussian functions to model the probability distribution of three tissue classes, which can be seen as fuzzy membership functions with Gaussian shapes. Therefore, the final probabilities of belonging of each voxel to a particular tissue class produced by this segmentation algorithm can be treated as fuzzy membership values.

Until now, two kinds of information are available for segmentation purpose: one is the prior knowledge of intensity, spatial location, and relative spatial relations of one structure l , rendered by the registered fuzzy templates \tilde{A}^l, \tilde{B}^l and \tilde{T}^l ; the other one is from the tissue segmentation of the test image itself denoted by $P = (P_i^k: i \in I, k = \{GM, WM, CSF\})$, where P_i^k stands for the probability of belonging to tissue class k and its value is in the range $[0, 1]$. Since the total fuzzy template \tilde{T}^l consists of all information in three feature templates, combining it with the tissue data P is an effective way to produce a more accurate fuzzy membership map of structure l in the test image f . T-norm fusion operator is applied as follows:

$$K_i^l = \sqrt{\tilde{T}_i^l P_i^k} \text{ if structure } l \text{ contains tissue type } k. \quad (14)$$

where K_i^l is the fuzzy membership value giving the degree of belongingness of voxel i to the structure l .

Detection of the structures

Decision or defuzzification is required to decide on the belongingness of each voxel i to structure l in the test image f . For each voxel i , we find the structure l^* with maximum fuzzy membership among all structures of interests $l \in \Gamma$, then assign zero fuzzy membership value to all other structures $l(\neq l^*)$ for this voxel to avoid overlapping.

$$\text{If } l^* = \arg \max_{l \in \Gamma} K_i^l \text{ then let } K_i^l = 0 \text{ for } l \neq l^*. \quad (15)$$

We apply a simple α -cut thresholding technique to this final fuzzy map K as follows: Voxel i in image f belongs to structure class l if

$$K_i^l \geq \xi_l, \quad (16)$$

where the threshold ξ_l is automatically learned from all training images of structure l . The resulting group of voxels belonging to structure l is the surest group satisfying all the information above. In other words, structure l has been identified from test image f based on intensity, spatial location, relative spatial relations to the other structures, and tissue information.

Determination of the threshold

This section describes the procedure of determining the threshold ξ_l in Eq. (16) for detecting the structure l from a given test image f . Suppose a fuzzy template T^l was created from the set F of N training images in order to identify structure l . During training, an optimal threshold ξ_l^j for detecting the structure l in each training image f_j is learned by using the combined fuzzy map $K^{lj} = (K_i^{lj}: i \in I, j = 1, 2, \dots, N)$; the optimal threshold is then chosen in such a manner that the target structure is detected from the training image to have the highest mean of the volume difference and overlap indices by using the known manual segmentation as the ground truth. Each training image produces one optimal threshold, resulting in a set of thresholds $\{\xi_l^j: l \in \Gamma, j = 1, 2, \dots, N\}$. The confidence value of each threshold ξ_l^j is noted by weights $w_l^j = (I_1^j + I_2^j) / 2$. As I_1 defined in Eq. (17) and I_2 defined in Eq. (18) are both in the range $[0, 1]$, the confidence weights $\{w_l^j: l \in \Gamma, j = 1, 2, \dots, N\}$ are in the same range as well. The threshold ξ_l for detecting the structure l in a given test image f is determined by taking a weighted average of

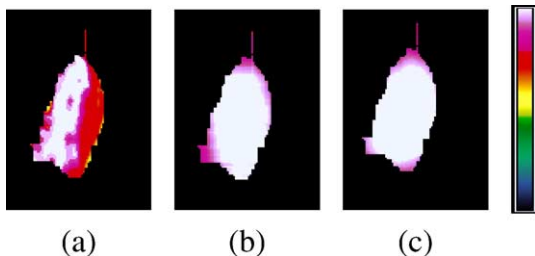


Fig. 1. Fuzzy feature maps of left thalamus on axial slice ($z = 155$) in one representative training image: (a) intensity fuzzy map; (b) spatial location fuzzy map; and (c) relative spatial relations fuzzy map. The color bar represents fuzzy membership range, in which the upper end represents one and the bottom end represents zero.

the set of thresholds, ξ_i^j , obtained for the training images, with their corresponding confidence weights, w_i^j .

Experimental results

Data

In our experiments, the MR brain images and their manual segmentations were obtained from the Center for Morphometric Analysis at Massachusetts General Hospital (IBSR, 2004). There are 18 images in this data set; one image was identified to have relatively large ventricle system and hence was removed from our analysis. Each of 17 T1-weighted volumetric images is composed of 128 coronal slices of 1.5 mm thick with 256×256 matrix per slice; voxel size is $0.94 \times 0.94 \times 1.5 \text{ mm}^3$. According to their documentation, these images have been positionally normalized into the Talairach coordinates (rotation only) and corrected for bias fields.

The standard reference template r for training image normalization is the single subject MRI anatomical brain template provided by International Consortium for Brain Mapping (ICBM, 2004). It has 362 coronal slices of 0.5 mm thick with 304×309 matrix per slice and a voxel size is $0.5 \times 0.5 \times 0.5 \text{ mm}^3$. Since our method is

voxel-based, this standard template provides a reference template or coordinate system to create fuzzy feature maps and to combine several features together for total fuzzy template.

Quantitative indices for validation

Three quantitative measures were used to evaluate the performance of our segmentation algorithm with reference to the expert segmentations (Iosifescu et al., 1997; Kelemen et al., 1999; Barra and Boire, 2001). Suppose that the true labeling of a structure l is denoted by l_t , the labeling produced by a segmentation algorithm is l_c , and the function $V(l)$ returns the volume or the number of voxels in the structure labeled l .

1. *Percent volume difference* is computed from the relative error in volume estimation when the true volume is given by the expert as:

$$I_1 = 1 - \frac{|V(l_t) - V(l_c)|}{V(l_t)} \tag{17}$$

2. *Percent overlap or spatial accuracy* assesses the relative overlapping of the computed structure l_c and the true one l_t as:

$$I_2 = \frac{V(l_t \cap l_c)}{V(l_t)} \tag{18}$$

3. *Mean distance* measures the absolute distance (in millimeters) of the computed structure to the true one, defined as:

$$I_3 = \frac{\sum_{c \in l_c} \min_{t \in l_t} \|c - t\|}{V(l_c)}, \tag{19}$$

where c represents a voxel in the detected structure l_c , and t represents a voxel in the true structure l_t ; $\|c - t\|$ stands for the distance between two voxels.

Perfect matching between the computed volume and true volume is achieved when the first two indices equal to one and the mean distance measure equals to zero. Note that some published results use the average volume of the predicted and manually labeling (Xue et al., 2000; Fischl et al., 2002) or the union of these two (Amini et al., 2004) as a normalization factor as opposed to manual labeling volume used here.

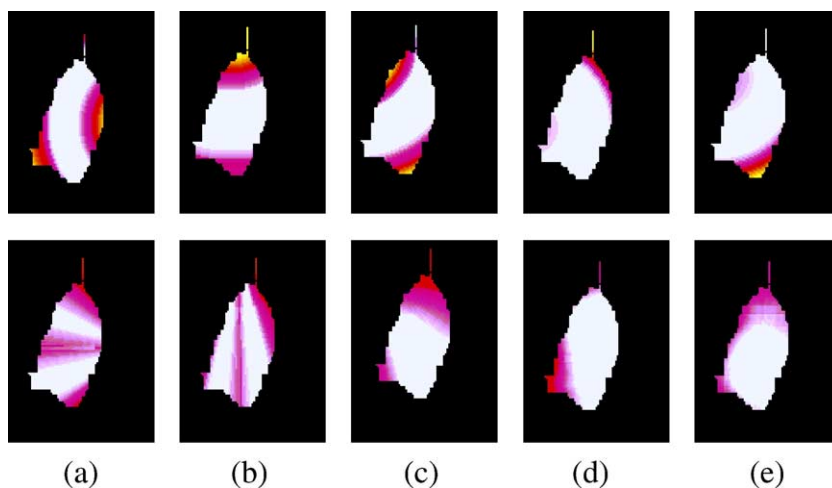


Fig. 2. Relative spatial relations fuzzy maps of left thalamus on axial slice ($z = 155$) in one training image. First row is relative distance fuzzy maps; second row is relative direction fuzzy maps. They are calculated relative to (a) right thalamus; (b) left caudate; (c) left putamen; (d) left hippocampus; and (e) left amygdala. The same color bar measure was used as in Fig. 1.

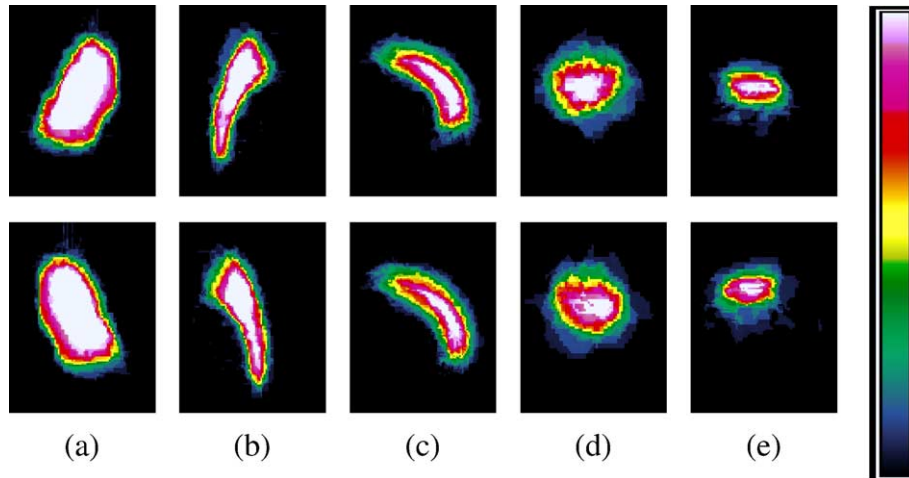


Fig. 3. Total fuzzy templates for 10 structures of interests: (a) thalamus, (b) putamen, (c) caudate, (d) hippocampus, and (e) amygdala. First row is structures in left brain and second row is structures in right brain. Thalamus (axial slice $z = 155$); putamen (axial slice $z = 136$); caudate (sagittal slice $x = 177$ for left and $x = 122$ for right); hippocampus (coronal slice $y = 184$); amygdala (axial slice $z = 103$). The color bar represents fuzzy membership range, in which the top end represents one and the bottom represents zero.

Creating fuzzy templates

In this section, the procedure of creating fuzzy templates as described in Construction of fuzzy templates is demonstrated with a set of training images. The whole process is in 3D, but some 2D slices are shown for illustration purposes. In this step, different fuzzy feature maps of structure l based on a single training image f_j are first calculated. For example, Fig. 1 presents (a) the intensity fuzzy map A_j^l , (b) the spatial location fuzzy map B_j^l , and (c) relative spatial relations fuzzy map C_j^l of structure l (left thalamus) for a representative training image f_j .

For creating relative spatial relations fuzzy map C_j^l as shown in Fig. 1(c), five reference structures are chosen for each target structure, which includes four other structures on the same side of the brain and the same target structure in the opposite side of the brain. For instance, if we want to obtain relative spatial relations fuzzy feature map about left thalamus, the corresponding reference structures are putamen, caudate, hippocampus, and amygdala in left brain and thalamus in right brain. Relative spatial relations are computed in terms of relative direction and relative distance. Fig. 2 shows relative distance (first row) and relative direction (second row) fuzzy maps with respect to five reference structures for structure l (left thalamus) in one representative training image. These fuzzy maps will be combined together by Eqs. (8)–(11) to form one fuzzy map representing relative spatial relations of left thalamus C_j^l for the training image f_j . Other nine structures follow exactly the same procedure to produce fuzzy maps.

After that, the fuzzy feature maps of all the training images are fused together to create a total fuzzy template of subcortical structures by Eqs. (12) and (13). Fig. 3 presents total fuzzy templates T^l , $l \in \Gamma$, for 10 structures including thalamus, putamen, caudate, hippocampus, and amygdala (both left and right).

Segmenting subcortical structures

In the fuzzy template of a certain structure, every voxel has a fuzzy membership representing its degree of belongingness to this structure. This kind of prior knowledge is used in the

segmentation step as described in Segmentation, and is fused with gray matter tissue fuzzy map since all five structures of interests contain gray matter tissue class. The final combined fuzzy map is able to roughly delineate the target structure. The decision is made to accurately identify the structure by first computing the structure with maximum belongingness for each voxel and then retaining voxels having a membership superior to a certain threshold ξ_i^{test} in the combined fuzzy map of structure l for the test image. The thresholding is done in three-dimensional space, and a technique to remove unconnected voxels is applied for final decision. As described in Determination of the threshold, the threshold for identifying structure l from the test image was automatically learned during the detection of structure l from all the training images.

Table 1

Quantitative evaluation of the segmentation of subcortical structures: best-case, worst-case, and average over 17 subjects

Structure	Index	Left			Right		
		Best	Worst	Mean	Best	Worst	Mean
Caudate	I_1	0.99	0.71	0.91 ± 0.07	0.88	0.85	0.90 ± 0.07
	I_2	0.80	0.82	0.81 ± 0.06	0.89	0.64	0.80 ± 0.08
	I_3	0.25	0.50	0.31 ± 0.11	0.26	0.55	0.32 ± 0.11
Putamen	I_1	0.98	0.72	0.91 ± 0.08	0.99	0.87	0.91 ± 0.08
	I_2	0.90	0.87	0.84 ± 0.06	0.84	0.68	0.81 ± 0.06
	I_3	0.13	0.57	0.25 ± 0.12	0.20	0.35	0.33 ± 0.12
Thalamus	I_1	0.95	0.88	0.95 ± 0.03	0.98	0.99	0.95 ± 0.03
	I_2	0.89	0.75	0.83 ± 0.05	0.88	0.69	0.84 ± 0.06
	I_3	0.23	0.22	0.32 ± 0.17	0.19	0.82	0.32 ± 0.19
Hippocampus	I_1	0.95	0.85	0.89 ± 0.09	0.95	0.89	0.88 ± 0.07
	I_2	0.86	0.60	0.72 ± 0.11	0.77	0.43	0.70 ± 0.11
	I_3	0.23	1.17	0.55 ± 0.27	0.37	1.21	0.56 ± 0.24
Amygdala	I_1	0.99	0.79	0.81 ± 0.17	0.99	0.76	0.78 ± 0.20
	I_2	0.72	0.36	0.66 ± 0.15	0.73	0.41	0.64 ± 0.15
	I_3	0.23	1.08	0.63 ± 0.25	0.39	1.03	0.70 ± 0.22

I_1 —percent volume difference, I_2 —percent volume overlap, and I_3 —mean distance for segmentation (mm); the best and worst cases were decided by the maximum and minimum values of the sum $I_1 + I_2$, respectively.

Cross-validation

In order to validate our approach, leave-one-out (LOO) cross-validation method was used on the data set of 17 images. In each round, the fuzzy templates were obtained by training 16 images and then tested on the left-out image. The results are evaluated by comparing to the manual segmentation in terms of three indices described in Quantitative indices for validation. Table 1 illustrates the best, worst, and average segmentation results for all 17 images in terms of three indices for 10 structures—thalamus, putamen, caudate, hippocampus, and amygdala (both left and right) detected by the present approach. Fig. 4 illustrates the best and worst segmentation results of all 10 structures on one brain slice by overlapping true volume and predicted volume together. Note that the experts did the manual segmentation in coronal slices, so the manual segmentation has smooth edges in coronal slices but chaotic edges in axial and sagittal slices. Because only selected slice is shown, some connected part of the structure may seem as unconnected.

A tradeoff between the indices I_1 and I_2 is observed; in other words, as the predicted volume is increasing, the percent volume

difference index I_1 and percent volume overlap index I_2 keep increasing, but when the predicted volume is larger than the true volume, I_1 starts to decrease. Different structures have different intensity, shape, size, and orientation variance. Therefore, the threshold learned from the training stage may not be the optimal one for the test image. Satisfying performance was achieved for thalamus, putamen, and caudate with very low mean distance error, which is less than 0.5 mm on average. This indicates that volume estimation is very consistent with respect to the expert quantification and there is a good match between expert segmentation and our segmentation results. Hippocampus and amygdala are rather small subcortical structures with large individual variations, so the segmentation accuracy still require improvement although the mean distance index was less than 1 mm in most cases.

Fig. 5 compares the present segmentation results in terms of average accuracy for all 10 structures with the approach presented by Iosifescu et al. (1997) using same indices (I_1 , I_2 , and I_3). Although the images used are different, we can still make some comparisons to see the potential of the present method. Their approach uses an elastic registration algorithm to a MRI brain atlas based on a single subject (Kikinis et al., 1996), but our method

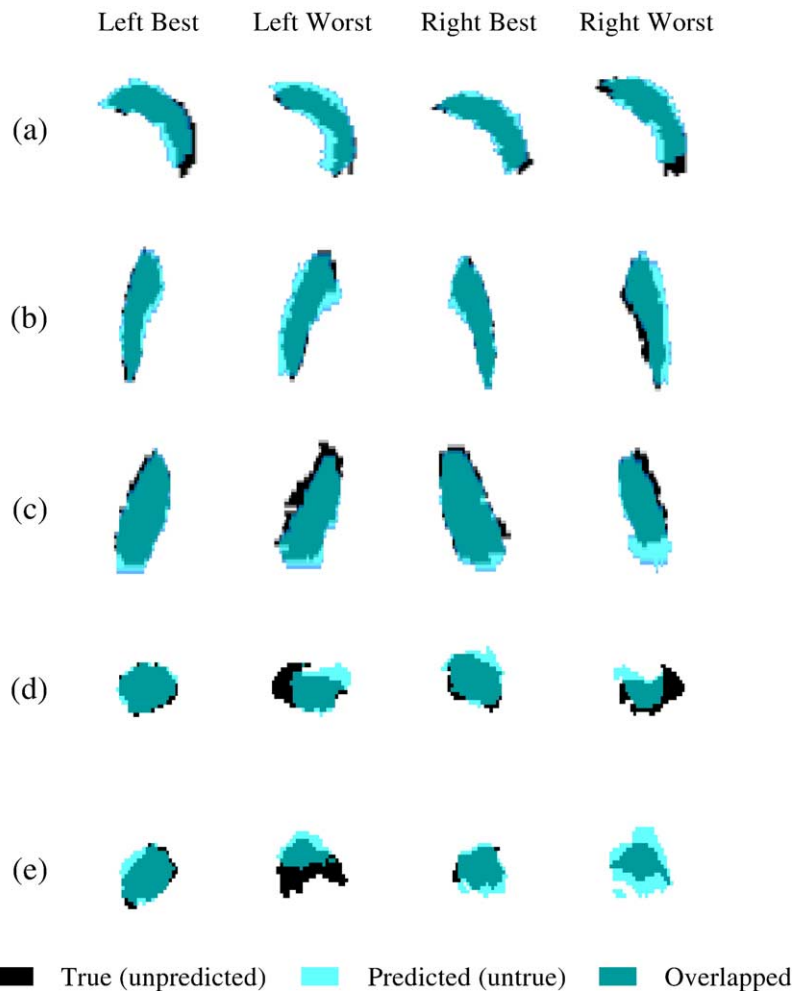


Fig. 4. Best and worst segmentation results with reference to manual segmentation for 10 structures on selected slices: (a) caudate (sagittal); (b) putamen (axial); (c) thalamus (axial); (d) hippocampus (coronal); and (e) amygdala (coronal). Columns (i) and (ii) show best and worst results for the structures in left brain, while columns (iii) and (iv) show best and worst results for the structures in right brain. The overlapped volume indicates where both the true volume and the predicted volume overlapped.

creates fuzzy templates from a set of training images. We have comparable performance for thalamus and better accuracy for putamen and caudate. In particular, the volume overlap index is much higher, so the significance of the use of the fuzzy templates is demonstrated. Furthermore, our approach could reasonably detect structures like amygdala and hippocampus. Our results for hippocampus are comparable to results of individual image shown in by Kelemen et al. (1999), where no average results are given.

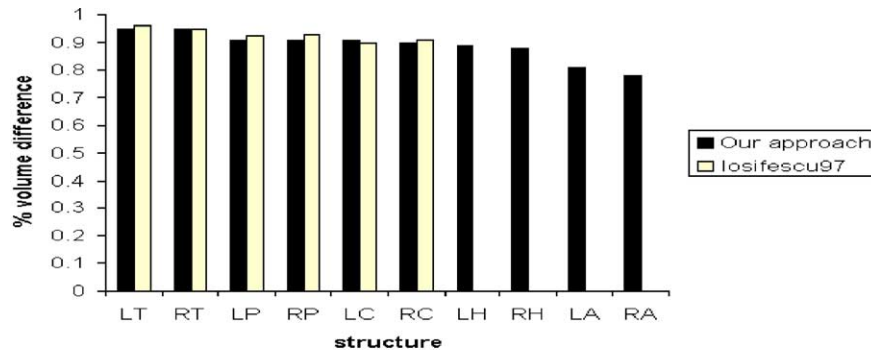
The method of Barra and Boire (2001), though based on a similar framework using fuzzy maps for the segmentation as ours, treats each structure individually by doing different fusion steps with reference to expert definitions. Similarly, in Barra et al. (2001), same framework is applied to segment subthalamic nucleus (ST). However, they first segmented the third ventricle (V3) and the two read nucleus (RN), and then identified subthalamic nucleus (ST) based on these neighboring structures by using topological information provided by expert and tissue information from the image. This procedure largely depends on whether the previous two neighboring structures are accurately identified. Moreover, some parameters in their expert definitions such as “25 mm” between two structures are quite vague and not general enough for other group of subjects. In short, we took an holistic approach for the detection of subcortical structures, in which all interested structures are detected simultaneously; dependence on previous segmentation is not required. However, an individualistic approach, such as Barra and Boire (2001), may turn out to be more accurate for volume overlap measure for one group of subjects for a particular structure, but may

not be accurate, in general, on other groups. Therefore, an objective comparison of our method with their approach is inappropriate.

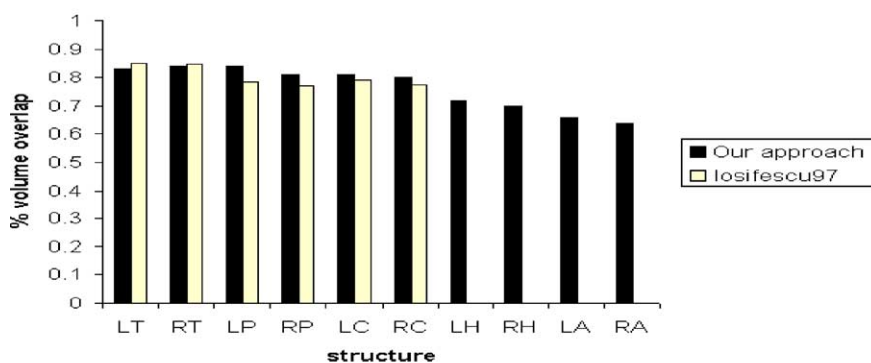
Registration artifacts

In our approach, registration step plays an important role in both training and testing. In order to evaluate the accuracy of the nonlinear registration algorithm and its effect to the performance of our approach, an experiment was designed involving the following two steps: (1) register a test image f and its expert segmentation s to a standard template r , say by transform H' , to obtain the normalized segmented images $\tilde{s} = H'(s)$; (2) register the same standard template r back to the test image by another transformation: $r = H(f)$, and apply it to \tilde{s} to get $\tilde{\tilde{s}} = H(\tilde{s})$.

If the nonlinear registration algorithm is able to perfectly match the target image f and the template r , different anatomical parts of the brain should be aligned accordingly although sampling errors still exist, in other words, $\tilde{\tilde{s}}$ approximates s nicely for each structure l . However, usually this may not be the case because of large individual variability and registration deformations. Therefore, for each structure of interest l , by comparing the expert segmentation s^l with the processed segmentation $\tilde{\tilde{s}}^l$, registration accuracy can be evaluated in terms of volume difference, volume overlap, and mean distance error as shown in Table 2. The registration error can be seen in terms of low volume difference, low volume overlap, and high mean distance error. Note that this registration error includes twice of the normalization step. The above process emulates the



(a) Percent volume differences of various structures



(b) Percent volume overlaps of various structures

Fig. 5. Performance comparison of the present approach and the approach of Iosifescu et al. (1997). Key: LT—left thalamus, RT—right thalamus, LP—left putamen, RP—right putamen, LC—left caudate, RC—right caudate, LH—left hippocampus, RH—right hippocampus, LA—left amygdala, RA—right amygdala.

Table 2

Quantitative evaluation of the registration effect on subcortical structures averaged over 17 subjects: I_1 —percent volume difference, I_2 —percent volume overlap, I_3 —mean distance, and $I_3^{r/s}$ —percentage of registration mean distance error divided by segmentation mean distance error

Structure	I_1	I_2	I_3 (mm)	$I_3^{r/s}$ (%)
Caudate (L)	0.64 ± 0.07	0.53 ± 0.06	0.22 ± 0.19	70.9
Caudate (R)	0.65 ± 0.08	0.54 ± 0.07	0.23 ± 0.22	71.8
Putamen (L)	0.75 ± 0.08	0.63 ± 0.07	0.21 ± 0.11	84.0
Putamen (R)	0.74 ± 0.07	0.61 ± 0.06	0.25 ± 0.13	75.7
Thalamus (L)	0.76 ± 0.08	0.69 ± 0.06	0.14 ± 0.11	43.8
Thalamus (R)	0.75 ± 0.08	0.68 ± 0.05	0.13 ± 0.12	40.6
Hippocampus (L)	0.63 ± 0.08	0.51 ± 0.09	0.25 ± 0.13	45.4
Hippocampus (R)	0.62 ± 0.07	0.49 ± 0.08	0.30 ± 0.16	53.5
Amygdala (L)	0.66 ± 0.09	0.47 ± 0.09	0.40 ± 0.18	63.4
Amygdala (R)	0.68 ± 0.08	0.46 ± 0.09	0.49 ± 0.21	70.0

normalization procedure involved in the training and testing stage of our method, so the errors and the information lost in the registration step influence our segmentation performance.

Because of this registration artifact, a simple mapping from a crisp segmented template to the target image does not satisfy for segmenting subcortical structure. The fuzzy templates in our approach encode the necessary anatomical information in a 3D fuzzy membership distribution, hence is able to adapt to the target image and identify the structure of interest better than crisp template after registration. Despite this, the registration still contributes to a significant amount of the segmentation error as shown in the fourth column $I_3^{r/s}$ of Table 2. The highest ratios occurred in detecting putamen (84.0% (L) and 75.7% (R)) and the lowest in thalamus (43.8% (L) and 40.6% (R)). The higher ratios reflect that the correct identification of particular structures relies more heavily on the registration procedure. Despite the heavy dependence on the registration procedure, the overall accuracies of the detection of subcortical structures from our algorithm were acceptable. However, more intelligent registration algorithms creating more accurate fuzzy templates of these structures and enhancing the fuzzy templates' ability to adopt to a particular image will certainly improve the accuracy of our approach.

Further, because of the nonlinear transformation used in the registration procedure, some voxels that belong to one structure in the original manual segmentation are seen as outliers on the final registered version of this structure. A connected component technique was used in our approach to remove such unconnected voxels in each structure as a post-processing step to registration.

Discussion and conclusion

A novel method for the segmentation of brain subcortical structures was presented, which constructs fuzzy templates for different structures based on the information extracted from a set of training images. Important features such as intensity, spatial location, and relative spatial relations were considered and fused together. Fuzzy templates are registered to a given test image and further fused with its tissue information to produce fuzzy memberships of different structures. The final fuzzy maps successfully segment thalamus, putamen, caudate, hippocampus, and amygdala in 17 T1-weighted MR images. Our method showed comparable or better results compared to the previous approaches

as evidenced by the quantitative measures: percent volume difference, percent volume overlap, and mean distance.

The method is based on a holistic framework involving intensity, spatial location, relative spatial relations, and tissue features, and no specific expert definitions of structures or interventions during the process are required because the prior knowledge was automatically extracted from the training data. The fuzziness of the maps captures the variability of each structure in the group of test images; several fuzzy feature templates and new information from the test image itself can be incorporated nicely. Hence, it is possible to generalize our approach to other structures or to other image data.

There are also some limitations of our method. The segmentation performance of one test image depends on the prior knowledge of the fuzzy template derived from training images. Because intensity, spatial location, and relative spatial relations vary among different group of subjects, and may change during development. For instance, intensity may change with age-dependent iron accumulation or myelination, spatial localization may vary with gender or other variables, and relative spatial relations may change during development. Hence, it is necessary to consider the population under study and the training images should be a good representation of the population. Moreover, according the experiment illustrated in Registration artifacts, registration step plays an important role both in training and testing stage of our approach. Any improvements of the registration could enhance the fuzzy template's ability to adapt to a particular image and improve the accuracy of our technique.

In this experiment, we demonstrated the segmentation of only five subcortical structures (left and right). For calculating relative spatial relations fuzzy template of one structure, we chose to assign four other structures on the same side and the same structure in opposite side of the brain as the reference structures. However, certain structure may not have reference structures in all directions, and this affects the accuracy of relative spatial relations fuzzy template. Further work may be necessary to include more representative structures in different directions as reference structures in order to increase the sensitivity of relative spatial relations fuzzy templates at the expense of the computation cost. Our method extracts tissue information from the test image and incorporates it with the prior knowledge to achieve high sensitive fuzzy map for segmentation. But certain subcortical structure like thalamus has diffuse gray level intensity, which makes the tissue segmentation inaccurate. A more intelligent tissue segmentation will enhance system performance (Rajapakse and Kruggel, 1998). Future work can extract more useful information, besides the tissue type information, from the test image itself to detect each subject's own uniqueness and subtle shape changes. Here, fuzzy templates are created based on T1-weighted images only. Multiple channel images include more than one MRI property of tissues, so it is possible to enhance discriminating power by incorporating new information, such as tissue or intensity fuzzy memberships, from other multi-spectral images (Rajapakse et al., 1996). As seen in the experiments, the accuracy of our segmentation approach could be greatly enhanced by improving the registration technique.

References

- Amini, L., Soltanian-Zadeh, H., Lucas, C., Gity, M., 2004. Automatic segmentation of thalamus from brain MRI integrating fuzzy clustering and dynamic contours. *IEEE Trans. Biomed. Eng.* 51 (5), 800–811.

- Ashburner, J., Friston, K., 1997. Multimodal image coregistration and partitioning—A unified framework. *NeuroImage* 6 (3), 209–217.
- Ashburner, J., Friston, K., 1999. Nonlinear spatial normalization using basis functions. *Hum. Brain Mapp.* 7 (4), 254–266.
- Ashburner, J., Friston, K., 2000. Voxel-based morphometry—The methods. *NeuroImage* 11, 805–821.
- Ashburner, J., Neelin, P., Collins, D.L., Evans, A., Friston, K., 1997. Incorporating prior knowledge into image registration. *NeuroImage* 6, 344–352.
- Barra, V., Boire, J., 2001a. Automatic segmentation of subcortical brain structures in MR images using information fusion. *IEEE Trans. Med. Imaging* 20 (7), 549–558.
- Barra, V., Lemarie, J., Durif, F., Biore, J., 2001b. Segmentation of the subthalamic nucleus in MR images using information fusion—A preliminary study for a computed-aided surgery of Parkinson's disease. *MICCAI 2001* 1183–1184.
- Fischl, B., Salat, D.H., Busa, E., Albert, M., Dieterich, M., Haselgrove, C., van der Kouwe, A., Killany, R., Kennedy, D., Klaveness, S., Montillo, A., Makris, N., Rosen, B., Dale, A.M., 2002. Whole brain segmentation: automated labeling of neuroanatomical structures in the human brain. *Neuron* 33, 341–355.
- Friston, K.J., Ashburner, J., Frith, C.D., Poline, J.-B., Heather, J.D., Frackowiak, R.S.J., 1995. Spatial registration and normalization of images. *Hum. Brain Mapp.* 2, 165–189.
- International Consortium of Brain Mapping (ICBM), 2004. ICBM single subject MRI brain template, http://www.loni.ucla.edu/ICBM/ICBM_BrainTemplate.html.
- Internet Brain Segmentation Repository (IBSR), the Center for Morphometric Analysis at Massachusetts General Hospital, 2004. MR brain images and their manual segmentations, <http://www.cma.mgh.harvard.edu/ibsr/>.
- Iosifescu, D.V., Shenton, M.E., Warfield, S.K., Kikinis, R., Dengler, J., Jolesz, F.A., McCharley, R.W., 1997. An automated registration algorithm for measuring MRI subcortical brain structures. *NeuroImage* 6, 13–25.
- Kelemen, A., Szekely, G., Gerig, G., 1999. Elastic model-based segmentation of 3-D neuroradiological data sets. *IEEE Trans. Med. Imaging* 18, 828–839.
- Kikinis, R., Shenton, M.E., Iosifescu, D.V., McCharley, R.W., Saiviroonporn, P., Hokama, H.H., Robatino, A., Metcalf, D., Wible, C.G., Portas, C.M., Donnino, R.M., Jolesz, F.A., 1996. A digital brain atlas for surgical planning, model driven segmentation, and teaching. *IEEE Visual. Comput. Graph.* 2 (3), 232–241.
- Magnotta, V.A., Heckel, D., Andreasen, A.C., Cizaldo, T., Corson, P.W., Ehrhardt, J.C., Yuh, W.T., 1999. Measurement of brain structures with artificial neural networks: two- and three-dimensional applications. *Radiology* 211, 781–790.
- Mangin, J.F., Poupon, F., Duchesnay, E., Riviere, D., Cachia, A., Collins, D.L., Evans, A.C., Regis, J., 2004. Brain morphometry using 3 D moment invariants. *Med. Image Anal.* 8, 187–196.
- Pham, D.L., Xu, C., Prince, J.L., 2000. Current methods in medical image segmentation. *Annu. Rev. Biomed. Eng.* 2, 315–338.
- Pitiot, A., Delingette, H., Thompson, P.M., Ayache, N., 2004. Expert knowledge-guided segmentation system for brain MRI. *NeuroImage* 23, S85–S96.
- Rajapakse, J.C., Kruggel, F., 1998. Segmentation of MR images with intensity inhomogeneities. *Image Vision Comput.* 16, 165–180.
- Rajapakse, J.C., DeCarli, C., McLaughlin, A., Giedd, J.N., Krain, A.L., Hamburger, S.D., Rapoport, J.L., 1996. Cerebral magnetic resonance image segmentation using data fusion. *J. Comput. Assist. Tomogr.* 20 (2), 206–218.
- Rajapakse, J.C., Giedd, J.N., Rapoport, J.L., 1997. Statistical approach to segmentation of single-channel cerebral MR images. *IEEE Trans. Med. Imaging* 16 (2), 176–186.
- Sonka, M., Fitzpatrick, J.M., 2000. Handbook of medical imaging. *Med. Image Process. Anal.*, vols. 1 and 2. SPIE Press, pp. 69–211.
- Sonka, M., Tadikonda, S.K., Collins, S.M., 1996. Knowledge-based interpretation of MR brain images. *IEEE Trans. Med. Imaging* 15 (4), 443–452.
- Worth, A.J., Makris, N., Patti, M.R., Goodman, J.M., Hoge, E.A., Caviness, V.S., Kennedy, D.N., 1998. Precise segmentation of the lateral ventricles and caudate nucleus in MR brain images using anatomically driven histograms. *IEEE Trans. Med. Imaging* 17 (2), 303–309.
- Xue, J., Ruan, S., Moretti, B., 2000. Fuzzy modeling of knowledge for MRI brain structure segmentation. *ICIP00 I*, 617–620.
- Yang, C.J., Tagare, H.D., Staib, L.H., Duncan, J.S., 2004. Segmentation of 3 D deformable objects with level set based prior models. *Proc. IEEE International Conference of Biomedical*, pp. 85–88.